THE JOURNAL OF PHYSICAL CHEMISTRY C
A JOURNAL OF THE AMERICAN CHEMICAL SOCIETY

pubs.acs.org/JPCC

Article

Contributions of Charge Generation Versus Transport to Photocurrent in Dilute-Donor Organic Solar Cells with Non-fullerene Acceptors

Boya Zhang, Justin C. Bonner, Weijie Xu, Robert T. Piper, Lakshmi N. S. Murthy, and Julia W. P. Hsu*

Cite This: *J. Phys. Chem. C* 2022, 126, 20793−20799

Read Online

ACCESS | Metrics & More | Article Recommendations | Supporting Information

ABSTRACT: The photocurrent generation in dilute donor organic solar cells (DDOSCs) based on fullerene and non-fullerene acceptors is compared. The donor concentration is kept under 5 wt % to avoid the formation of a percolation pathway for hole transport, as verified by studying the hole mobilities in an insulating polymer matrix. The short-circuit current densities (J_{sc}) in DDOSCs for three common acceptors are quantified in terms of charge generation, transport, and collection, which are probed using ideal J_{sc} calculated from the transfer matrix method, hole mobility measured from space charge limited current method, and charge collection efficiency, respectively. Using non-fullerene acceptors improves both charge generation and transport, with charge transport being more important in determining J_{sc} in DDOSCs.

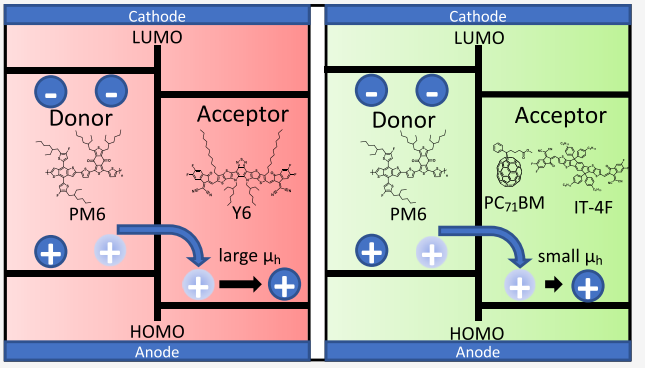

1. INTRODUCTION

Dilute donor organic solar cells (DDOSCs), which have active layers containing a low concentration of donor molecules in an acceptor matrix, are intriguing because they can achieve a high open-circuit voltage (V_{oc}) and a high short-circuit current density (J_{sc}) simultaneously.[1−5] Most DDOSC research utilizes fullerene-based acceptors.[2,4,6−11] However, fullerene-based acceptors have low optical absorption in the visible region[12] and low hole mobility,[6] both detrimental to photocurrent generation. In contrast, several non-fullerene acceptors (NFAs) exhibit strong absorption across a larger portion of the solar spectrum[13] and high mobilities with ambipolar characteristics.[14] These traits can facilitate better charge generation and transport in DDOSCs. However, to our knowledge, only two publications studied NFAs in DDOSCs.[15,16] While they reported good organic solar cell (OSC) performance, neither one explored the extreme dilute region—donor concentration ≤5 wt %—where donor molecules are likely to be isolated from each other and charge generation and carrier transport depend more on the acceptor's characteristics.

In this work, we compare DDOSCs that contain ≤5 wt % of poly[(2,6-(4,8-bis(5-(2-ethylhexyl-3-fluoro)thiophen-2-yl)-benzo[1,2-*b*:4,5-*b*′]dithiophene))-*alt*-(5,5-(1′,3′-di-2-thienyl-5′,7′-bis(2-ethylhexyl)benzo[1′,2′-*c*:4′,5′-*c*′]dithiophene-4,8-dione))] (PM6) donor molecules in three commonly used acceptor materials: [6,6]-phenyl-C_{71}-butyric acid methyl ester ($PC_{71}BM$)—representing fullerene-based acceptors—and two NFAs, 2,2′-((2*Z*,2′*Z*)-((12,13-bis(2-ethylhexyl)-3,9-diundecyl-12,13-dihydro-[1,2,5]thiadiazolo[3,4-*e*]thieno[2″,3″:4′,5′]-thieno[2′,3′:4,5]pyrrolo[3,2-*g*]thieno[2′,3′:4,5]thieno[3,2-*b*]-indole-2,10-diyl)bis(methanylylidene))bis(5,6-difluoro-3-oxo-2,3-dihydro-1*H*-indene-2,1-diylidene))dimalononitrile (Y6) and 2,2′-[[6,6,12,12-tetrakis(4-hexylphenyl)-6,12-dihydrodithieno[2,3-*d*:2′,3′-*d*′]-sindaceno[1,2-*b*:5,6-*b*′]-dithiophene-2,8-diyl]bis[methylidyne(5,6-difluoro-3-oxo-1*H*-indene-2,1(3*H*)-diylidene)]]bis[propanedinitrile] (IT-4F). Their chemical structures are shown in Figure 1. The choice of Y6 is motivated by the excellent device performance Yao et al.[16] reported for 10 wt % PM6 in Y6 and the high power conversion efficiency (PCE) of PM6:Y6 bulk heterojunction (BHJ) OSCs, 13.5−17.9%.[16−19] PM6:IT-4F BHJ OSCs also have high PCE values, 12.9−14.4%,[20−23] but IT-4F has different absorption and transport properties from Y6; thus, comparing Y6- and IT-4F-based DDOSCs will elucidate the role of the NFAs. We examine charge generation, transport, and collection based on experiments and numerical simulations. Understanding critical factors that govern photocurrent generation is pivotal for advancing NFA-based DDOSCs.

Received: November 6, 2022
Revised: November 15, 2022
Published: December 1, 2022

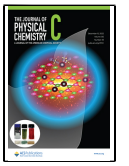

https://doi.org/10.1021/acs.jpcc.2c07821
J. Phys. Chem. C 2022, 126, 20793−20799

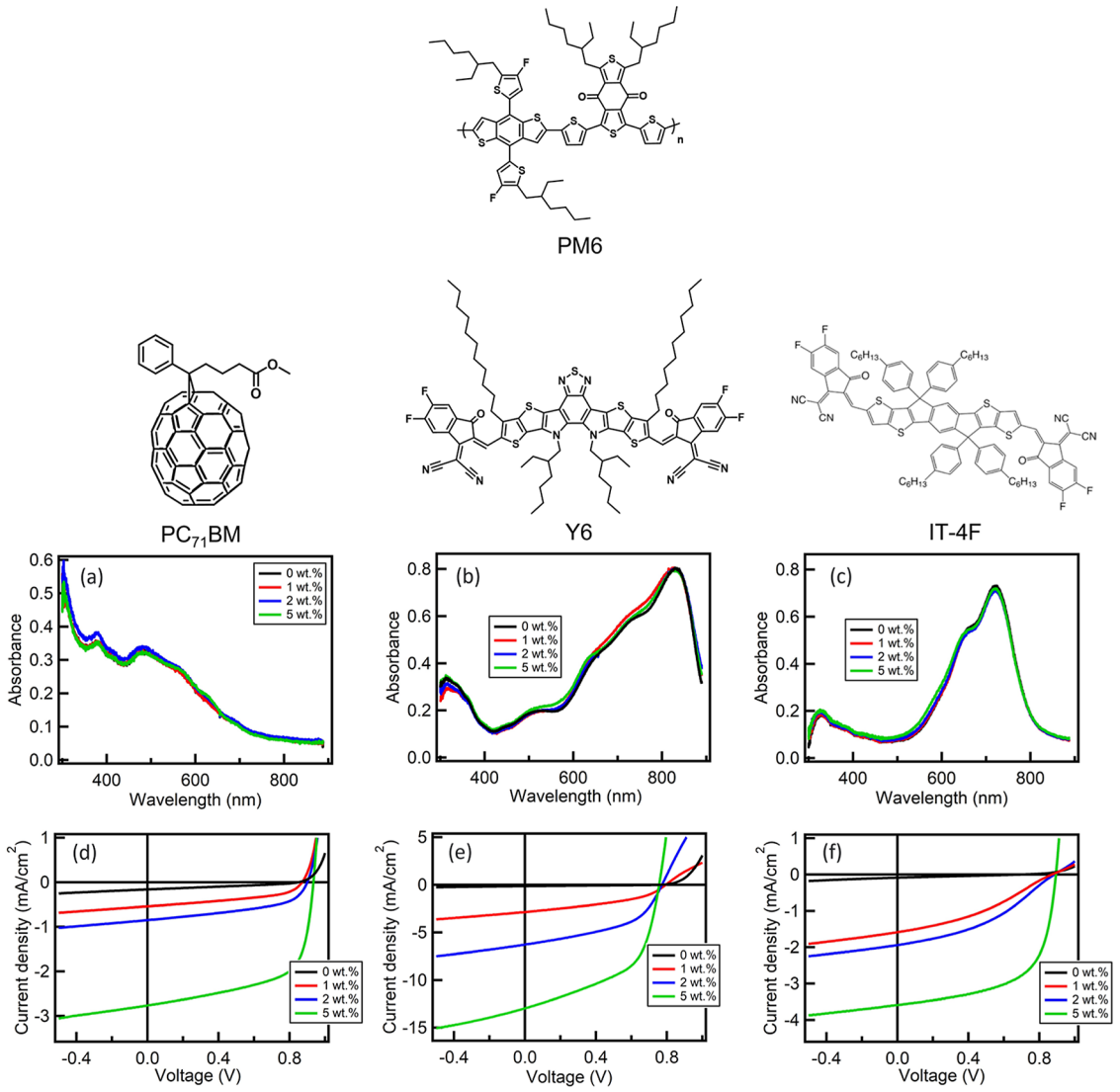

Figure 1. Absorbance spectra of (a) PM6:$PC_{71}BM$, (b) PM6:Y6, and (c) PM6:IT-4F active layers. The chemical structure of the donor is shown in the top row, and those of the acceptor materials are shown above the corresponding absorption spectra. $J-V$ curves of (d) PM6:$PC_{71}BM$, (e) PM6:Y6, and (f) PM6:IT-4F DD devices under 1 sun AM 1.5G 100 mW/cm^2 illumination. These $J-V$ curves are averaged over at least five devices for each type. The color schemes for all panels are 0 wt % (black), 1 wt % (red), 2 wt % (blue), and 5 wt % (green) PM6 in the acceptors.

2. METHODS

2.1. Materials. Y6, IT-4F, and $PC_{71}BM$ were purchased from Lumtec. Polymethyl methacrylate (PMMA) was purchased from Sigma-Aldrich, and poly(3-hexylthiophene) (P3HT) was purchased from Rieke Metals. Poly(4,8-bis(5-(2-ethylhexyl)furan-2-yl)benzo[1,2-*b*:4,5-*b*′]difuran-*alt*-2,5-didodecyl-3,6-di(furan-2-yl)pyrrolo[3,4-*c*]pyrrole-1,4(2*H*,5*H*)-dione) (PBDF-FDPP),[24] poly(2,5-bis(2-decyltetradecyl)-3,6-di(thiophen-2-yl)pyrrolo[3,4-*c*]pyrrole-1,4(2*H*,5*H*)-dione-*b*-(*E*)-1,2-di(furan-2-yl)ethene) (PThDPP-FVF),[25] and nitrogen-bridged terthiophene core with rhodanine (NBTT-Rho) small molecules[9,26] were synthesized and reported by published literature studies.

2.2. Device Fabrication. Conventional devices are fabricated with the structure glass/ITO/hole transport layer (HTL)/active layer/Ca/Al. Patterned ITO-coated glass substrates (Kintec, 15 Ω/sq) were rinsed with water and isopropanol and then treated with UV ozone (ProCleaner Plus, Bioforce Nanosciences) for 20 min. Poly(3,4-ethylenedioxythiophene):poly(styrenesulfonate) (Heraeus Clevios P VP.AI 4083, batch: 9006378404) was spin-coated onto precleaned glass/ITO substrates at 4000 rpm for 30 s, followed by 170 °C annealing in N_2 for 10 min to form ∼30 nm HTL. For current density−voltage ($J-V$) measurements, we first prepared the dilute donor (DD) PM6:Y6 solutions in chloroform (CF, Sigma-Aldrich) with donor concentrations of 0 and 10 wt %; then we mixed the two appropriately to obtain solutions of other donor concentrations (1, 2, and 5 wt %). These solutions, with a total concentration of 10 mg/mL, were stirred overnight at 50 °C. The active layers were made by spin-coating the prepared solutions at 700−1100 rpm for 60 s. Additional 5 wt % Y6 DD devices were made with donors (P3HT, NBTT-Rho, PBDF-FDPP, and PThDPP-FVF); the solutions were prepared the same to PM6:Y6 DD solutions. PM6:IT-4F DD active layer solutions were prepared similar to PM6:Y6 DD solutions, but the PM6:IT-4F solutions were in chlorobenzene (CB, Sigma-Aldrich) and had a total concentration of 20 mg/mL. The PM6:IT-4F active layers were made by spin-coating the prepared solutions at 1250−1700 rpm for 60 s, followed by annealing at 100 °C in N_2 for 10 min.

https://doi.org/10.1021/acs.jpcc.2c07821
J. Phys. Chem. C 2022, 126, 20793−20799

Table 1. Device Parameters of PM6:$PC_{71}BM$, PM6:Y6, and PM6:IT-4F Devices with 0−5 wt % PM6 Concentration[a]

acceptor	PM6 concn (wt %)	V_{oc} (V)	J_{sc} (mA/cm^2)	FF	PCE (%)
$PC_{71}BM$	0	0.83 ± 0.05	0.16 ± 0.00	0.30 ± 0.03	0.04 ± 0.00
	1	0.87 ± 0.01	0.55 ± 0.01	0.45 ± 0.01	0.22 ± 0.01
	2	0.90 ± 0.01	0.94 ± 0.03	0.50 ± 0.01	0.42 ± 0.02
	5	0.94 ± 0.01	2.85 ± 0.10	0.63 ± 0.01	1.67 ± 0.08
Y6	0	0.76 ± 0.01	0.15 ± 0.00	0.29 ± 0.00	0.03 ± 0.00
	1	0.78 ± 0.01	2.91 ± 0.11	0.47 ± 0.01	1.08 ± 0.05
	2	0.77 ± 0.01	4.27 ± 0.44	0.44 ± 0.03	1.44 ± 0.25
	5	0.76 ± 0.01	13.3 ± 0.40	0.48 ± 0.03	4.83 ± 0.42
IT-4F	0	0.71 ± 0.06	0.09 ± 0.00	0.25 ± 0.00	0.02 ± 0.00
	1	0.88 ± 0.01	1.60 ± 0.06	0.36 ± 0.00	0.50 ± 0.02
	2	0.89 ± 0.01	1.95 ± 0.05	0.39 ± 0.00	0.67 ± 0.02
	5	0.90 ± 0.00	3.60 ± 0.18	0.61 ± 0.00	1.97 ± 0.09

[a]The standard deviations are calculated from at least five devices for each type.

PM6:$PC_{71}BM$ DD solutions with 0−5 wt % PM6 were in CB with a total concentration of 20 mg/mL. The solutions were stirred overnight at 70 °C. The active layers were made by spin-coating the prepared solutions at 1300 rpm for 60 s, followed by annealing at 70 °C in N_2 for 10 min. For devices used in hole mobility measurements, the active layers are thicker than those devices for $J-V$ measurements to minimize electrical shorting. In addition, we made DD PM6:PMMA devices. The solutions, with 20 mg/mL total concentration, were dissolved in CB and stirred at 50 °C overnight. The active layers were made by spin-coating the prepared solution at 1000 rpm for 60 s. Except for PM6:PMMA hole-only devices, the thicknesses of the rest devices are obtained by fitting the absorbance spectra of the OSCs (Figure 1a−c) with the optical constants measured by ellipsometry as described below in Section 2.3. Finally, 7 nm Ca and 100 nm Al were thermally evaporated (Angstrom Engineering) on top of the active layer to complete the solar cells. For hole-only devices, MoO_3 (10 nm) and Ag (100 nm) were deposited as the top electrode instead of Ca and Al.

2.3. Materials Characterization. The measurement of the ultraviolet−visible (UV−vis) absorbance spectra of donor and acceptor thin films is performed using an Ocean Optics 4000 spectrometer with a DT-mini-2-GS light source. The measurement of the ionization energy is performed using photoelectron spectroscopy in air (PESA, RKI Instruments AC2) with 100 nW deuterium lamp power. The energy step in PESA measurements is 0.05 eV.

The spectroscopic ellipsometry measurements (M-2000DI, J. A. Woollam) were performed from 190 to 1690 nm at 55, 65, and 75° incident angles on all DD films prepared on top of glass substates. Reflection and transmission data for PM6:$PC_{71}BM$ and PM6:Y6 while only reflection data for PM6:IT-4F were obtained. PM6:$PC_{71}BM$ data were fitted using a B-spline model, and a thickness uniqueness test was completed to ensure accurate refractive index (n) and extinction coefficient (k) values. PM6:Y6 data were fitted using the uniaxial model because B-spline model produced a poor match to the experimental results. The uniaxial model for PM6:Y6 used φ, θ, and roughness parameters to get sensible n and k values. The B-spline model was used for PM6:IT-4F to find n and k values. Kramers Kronig relationship and the transparent region were analyzed first to find the best fit in each case.

For photoluminescence, samples were excited by a 485 nm pulsed diode laser (DD-485L, Horiba) with a repetition rate of 100 MHz. The emission was filtered through a 525 nm long-pass filter and a spectrometer (Horiba, iHR-320).

2.4. Device Characterization. The $J-V$ measurements were performed in a N_2-filled glovebox under AM 1.5G 100 mW/cm^2 illumination from a class AAA solar simulator (Abet Technologies) using a low-noise sourcemeter (2635A, Keithley). The solar simulator intensity was calibrated using a NIST-traceable Si photodiode (Abet RR_227KG5). A 2.5 mm diameter aperture was placed in front of each device to define the illuminated area of 0.049 cm^2. Hole mobility measurements were performed on the hole-only devices by biasing from 0 to 10 V in the dark.

3. RESULTS AND DISCUSSION

Figure 1a−c shows the absorbance of PM6:$PC_{71}BM$, PM6:Y6, and PM6:IT-4F active layers for PM6 concentration varying from 0 to 5 wt %. For all three acceptors, the DD absorbance spectra resemble the neat acceptor's spectrum because of the extremely low concentration of the donor. PM6:$PC_{71}BM$ primarily absorbs below 600 nm, while PM6:Y6 absorbs in 600−900 nm and PM6:IT-4F absorbs in 600−800 nm. Figure 1d−f shows the corresponding current density−voltage ($J-V$) curves under 1 sun AM 1.5G illumination of the DDOSCs. Table 1 contains the $J-V$ parameters. The PCE values reported in our paper are among the highest for solution-processed DDOSCs with donor concentrations ≤5 wt %. The PCE of our 5 wt % PM6:Y6 devices is 4.8%, which is slightly higher than that reported by Yao et al.[16] However, PCE is not the main focus of this paper. Instead, we aim to understand the mechanism(s) of photocurrent generation at extremely low donor concentrations. In addition, the different V_{oc} values are determined by the acceptor alone according to radiative and non-radiative recombination.[27]

OSCs with neat acceptors as the active layer, that is, 0 wt %, produce very low J_{sc}, 0.1 to 0.2 mA/cm^2. Figure 2 shows that with the addition of small amounts of PM6 donor, all three systems exhibit dramatic J_{sc} enhancement, which increases with increasing donor concentration. Spectacularly, adding 1 wt % PM6 in Y6 increases the J_{sc} by a factor of ∼20. For 5 wt % PM6:Y6 devices, J_{sc} is ∼90 times larger than that of the neat Y6 devices, increasing from 0.15 to 13 mA/cm^2. For 5 wt % PM6:IT-4F devices, J_{sc} increases by a factor of 40, from 0.09 to 3.60 mA/cm^2, and for 5 wt % PM6:$PC_{71}BM$, J_{sc} increases by 18 times from 0.16 to 2.85 mA/cm^2. We would like to point out that J_{sc} enhancement with small amounts of donors is not unique to PM6 being the donor or specific acceptors. Various

https://doi.org/10.1021/acs.jpcc.2c07821
J. Phys. Chem. C 2022, 126, 20793−20799

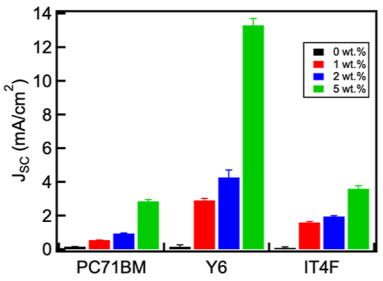

Figure 2. J_{sc} vs PM6 concentration in PM6:$PC_{71}BM$, PM6:Y6, and PM6:IT-4F devices for 0 wt % (black), 1 wt % (red), 2 wt % (blue), and 5 wt % (green) PM6 concentrations. The error bars represent one standard deviation of the measured devices.

donors in $PC_{71}BM$ have been reported previously.[6,8,9] We have included other donors in Y6 in the Supporting Information (Figure S1 and Table S1). All donors enhance photocurrent production in DDOSCs. The enhancement has been attributed to additional light absorption from the donor, increasing donor/acceptor interfacial areas to facilitate exciton dissociation, or the formation of percolation pathways to transport holes to the anode.[6,8,16] However, there has not been any study comparing J_{sc} dependence with different acceptors. Figure 2 and Table 1 show differences among the three acceptors. At a given PM6 concentration, PM6:Y6 DDOSCs produce significantly larger J_{sc} than the other two acceptor systems, while PM6:IT-4F DDOSCs generate slightly larger J_{sc} than the PM6:$PC_{71}BM$ system. To elucidate the acceptor roles, we next examine charge generation, transport, and collection, the governing factors that determine J_{sc}.[6,8,16,28]

To study charge generation in the different acceptors, we perform transfer matrix method (TMM) calculations[29,30] for all three DD systems using complex optical constants measured by spectroscopic ellipsometry (Figure S2). The thickness of the active layer is determined by matching the absorbance spectra of PM6:acceptors calculated from TMM with experimentally measured UV−vis spectra (Figure 1a−c) and shown in Table S2. The wavelength in the TMM simulation is 300−800 nm for PM6:$PC_{71}BM$ or 300−1100 nm for PM6:Y6/IT-4F using n and k values determined from ellipsometry. Then, we calculate the volumetric generation rate profile as a function of active layer position (Figure S2c,f,i). Figure 3 shows the areal generation rate, integrated over the active layer thickness, as a function of PM6 concentration in the three acceptors. It is evident that at every PM6 concentration, the generation is the lowest when the acceptor is $PC_{71}BM$, followed by IT-4F, and the highest for Y6

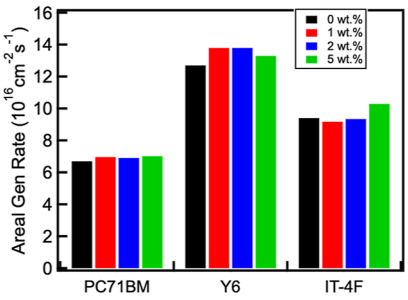

Figure 3. Areal generation rate calculated from TMM in $PC_{71}BM$, Y6, and IT-4F DDOSCs for 0 wt % (black), 1 wt % (red), 2 wt % (blue), and 5 wt % (green) PM6 concentrations.

DDOSCs. The difference can be explained in part by the lower absorption of $PC_{71}BM$ between 600 and 800 nm (Figure S2). For neat acceptor devices (0 wt %), the generation rate does not correspond to the measured J_{sc} (Table 1). Furthermore, for a given acceptor system, the generation rate does not substantially increase when donors are added into the acceptor matrix (comparing 0 to 1−5 wt % in Figure 3) for all three systems. Hence, generation cannot explain the observed J_{sc} shown in Figure 2.

To study charge transport, we first must understand the transport mechanism, which depends on donor morphology. If the donors aggregate and form a percolation path, as proposed for donor concentrations >10 wt %,[4,16,31] hole transport to the anode would be the same as in BHJ devices, that is, through the aggregated donor domains. As mentioned above, no NFA DD studies have been performed for donor concentrations <5 wt % previously. To examine whether the donor molecules form a percolative network or not, we first perform grazing angle X-ray diffraction (GIXRD) measurements on 5 wt % PM6:Y6 film. Figure S3a,b shows GIXRD patterns of neat PM6 and 5 wt % PM6:Y6 film, respectively. Zhu et al.[32] reported a peak at ∼4.6° for the neat PM6. However, we do not observe this peak in 5 wt % PM6:Y6 film, indicating little or no donor aggregation in the active layer to form a percolative pathway. We then adopt the method used in Yao et al. of measuring hole mobility of hole-only devices containing dilute PM6 in an insulating PMMA polymer matrix.[16] If the hole mobility increases substantially compared to neat PMMA, the donor molecules likely form a network to facilitate hole transport. If it is similar to the hole mobility of the neat PMMA, hole transport occurs via a different mechanism. We fabricated hole-only devices of neat PMMA and 1−5 wt % of PM6 in PMMA and extract hole mobility (μ_h) using the space charge limited current (SCLC) method described by Blakesley et al.[33] The details of data fitting and μ_h extraction are described in the Supporting Information (Figures S4−S7, Tables S3 and S4). As seen in Table S4, the μ_h value for the neat PMMA is 6.0×10^{-10} cm^2 V^{-1} s^{-1}, while the μ_h values of 1−5 wt % PM6 in PMMA are $(1-3) \times 10^{-9}$ cm^2 V^{-1} s^{-1}. Thus, we are in the isolated donor regime.

If the donors are isolated, but with a separation <4 nm, tunneling can contribute to photocurrent generation.[11] Modeling based on density functional theory showed that the donor−donor separation is too large at 1−2 wt % donor concentrations for tunneling to be the dominant hole transport mechanism, although tunneling can play a role for donor concentrations above 5 wt %.[6,11] For extremely low donor concentrations, where donors are isolated and far apart, hole back transfer[7] is the most plausible transport mechanism: (1) after excitons dissociate at the donor−acceptor interfaces, holes are first transferred to the donor phase; (2) with the accumulation of holes in an isolated donor domain, Coulomb repulsion overcomes the energy barrier associated with the offset between the donor's and acceptor's highest occupied molecular orbital (HOMO) levels and drives holes back to the acceptor domain; (3) holes are then transported to the anode through the acceptor matrix.

In the back transfer model, holes must transport through the acceptor matrix; therefore, we expect the hole mobility of the acceptor material to play an important role. We fabricate hole-only devices of three neat acceptors, $PC_{71}BM$, Y6, and IT-4F, and 1, 2, and 5 wt % of PM6 in these acceptors and extract μ_h using the same method described in the Supporting

https://doi.org/10.1021/acs.jpcc.2c07821
J. Phys. Chem. C 2022, 126, 20793−20799

Information. Figure S7 shows the representative SCLC fitting to the $J-V$ curves of hole-only PM6:$PC_{71}BM$, PM6:Y6, and PM6:IT-4F devices. Figure 4 and Table S4 show μ_h as a function of PM6 concentration. The μ_h values for the neat $PC_{71}BM$ and neat IT-4F are approximately the same, 1.9×10^{-9} cm^2 V^{-1} s^{-1}, while μ_h of the neat Y6 film is 5 orders of magnitude higher, 6.3×10^{-4} cm^2 V^{-1} s^{-1}. Given that holes are transported to the anode mostly via the acceptor matrix, we expect hole transport to be much more efficient in Y6 DD devices.

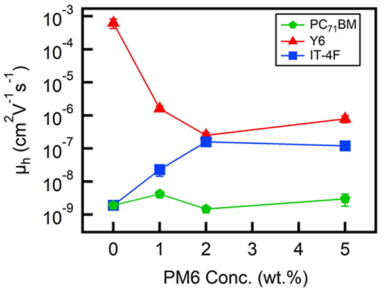

Figure 4. μ_h as a function of PM6 concentration for PM6:$PC_{71}BM$ (green diamond), PM6:Y6 (red triangle), and PM6:IT-4F (blue square). The standard deviations are calculated from at least three devices for each type.

With the addition of PM6, the μ_h behaviors are different depending on the acceptors. For the PM6:$PC_{71}BM$ system, μ_h variation is independent of PM6 concentrations and stayed in the 10^{-9} cm^2 V^{-1} s^{-1} range, similar to published results with other donors.[2,6] While the neat acceptors' μ_h values are the same for neat IT-4F and $PC_{71}BM$, adding PM6 causes the μ_h of PM6:IT-4F to increase to 1.2×10^{-7} cm^2 V^{-1} s^{-1} at 5 wt % PM6, approximately 2 orders of magnitude larger than μ_h of the 5 wt % PM6:$PC_{71}BM$ film. Interestingly, μ_h of the PM6:Y6 films decreases from 6.3×10^{-4} to 2.5×10^{-7} cm^2 V^{-1} s^{-1} as the PM6 content increases from 0 to 2 wt % (discussed below) and then increases to 7.9×10^{-7} cm^2 V^{-1} s^{-1} at 5 wt % PM6, which is still lower than μ_h for the neat Y6 but higher than μ_h of 5 wt % PM6:IT-4F and PM6:$PC_{71}BM$. The hole mobilities in 1−5 wt % Y6 (IT-4F) DDOSCs are 2−3 (1−2) orders of magnitude higher than those in $PC_{71}BM$ DDOSCs and produce 4−5 (2−3) times larger J_{sc} (Table 2). Thus, for DDOSCs with extremely low donor concentrations, the J_{sc} is dominated by charge transport. The only exception is for 2 wt % PM6:Y6 and PM6:IT-4F; because their μ_h values are similar, their J_{sc} values are then determined by the generation difference with PM6:Y6 being higher (Figure 3).

Table 2. J_{sc} Ratio between PM6:Y6 and PM6:$PC_{71}BM$ Devices as Well as J_{sc} Ratio between PM6:IT-4F and PM6:$PC_{71}BM$ Devices with 0−5 wt % PM6 Concentration

PM6 concn (wt %)	J_{sc} ratio (PM6:Y6/PM6:$PC_{71}BM$)	J_{sc} ratio (PM6:IT-4F/PM6:$PC_{71}BM$)
0	0.94	0.56
1	5.29	2.91
2	4.54	2.07
5	4.67	1.26

Since the non-monotonic donor concentration dependence of μ_h in the Y6 DD system is unusual, we fabricated hole-only devices to measure μ_h using two other donors (NBTT-Rho and PBDF-FDPP). The hole-only $J-V$ curves and μ_h values are shown in Figure S8 and Table S5. Adding donors at 5 wt % decreases μ_h in Y6 independent of donor materials. This is extremely surprising as no other donor:acceptor systems we know of display such a non-monotonic behavior. However, Yao et al. also reported a similar trend.[16] They did not study PM6 concentrations below 5 wt %, but their μ_h values for 5 and 10 wt % PM6:Y6 are lower than that of neat Y6. Only when the PM6 concentration increases to 20 wt %, the μ_h becomes comparable to that of neat Y6. We postulate that the reduction in μ_h in the PM6:Y6 system is caused by hole trapping inside PM6 donor sites. Due to the ambipolar characteristics of Y6, holes transport efficiently in the Y6 matrix. With a HOMO energy offset (ΔE_{HOMO}) of 0.52 eV (Figures S9 and S10), holes transfer from Y6 to PM6 readily after exciton dissociation. Due to the large ΔE_{HOMO}, the energy barrier for holes to transfer back to Y6 is too high and the holes are trapped in the donor domains.[7] Hence, the DD molecules act as traps in Y6 for holes, and hole mobility decreases. At 5 wt % PM6, the donor−donor separation distance begins to be small enough to facilitate tunneling, leading to μ_h increase, and aggregation of donors to form a percolation path becomes possible above 10 wt % PM6 concentration, further increasing μ_h. This explanation is consistent with our hole mobility results and those reported by Yao et al.[16]

To study the efficiency of charge collection in the different acceptors, we examine photocurrent density (J_{ph}, $J_{ph} = J_{light} - J_{dark}$) as a function of effective bias (V_{eff}, $V_{eff} = V_0 - V_{applied}$) for PM6:acceptors DDOSCs at different PM6 concentrations (Figure S11a−c), where V_0 is the voltage when J_{ph} is equal to 0.[34] Figure S11d shows the charge collection probability (P_C) as a function of PM6 concentration for DDOSCs with different acceptors. P_C is determined by dividing J_{ph} by the saturation photocurrent at sufficiently high V_{eff}.[34] At every PM6 concentration, the P_C values among different acceptors are similar. Therefore, charge collection in PM6:acceptors is independent of the acceptor. This is to be expected because charge collection depends strongly on the interfacial contact layers.[35] The hole and electron transport layers are the same in all DDOSCs.

4. CONCLUSIONS

We fabricate PM6-based DDOSCs with three commonly used acceptors, $PC_{71}BM$, Y6, and IT-4F, to probe photocurrent generation. We show that the photocurrent is the largest when the acceptor is Y6, followed by IT-4F, and the lowest for $PC_{71}BM$ DD at every PM6 concentration. With extremely low donor concentrations, ≤5 wt %, these DDOSCs are in the isolated donor regime with photocurrent generation largely governed by a hole back transfer mechanism. While charge collection is independent of the acceptors, both charge generation (Figure 3) and hole transport (Figure 4) contribute to J_{sc}, with the latter playing a more important role. Among the three systems, PM6:Y6 overall has the highest μ_h and much higher J_{sc}. The higher J_{sc} for DD PM6:IT-4F devices compared to PM6:$PC_{71}BM$ devices (Figure 2, Table 2) is consistent with the much higher μ_h of the PM6:IT-4F DDOSC devices. Our results indicate that NFAs are more promising for achieving high-efficiency DDOSCs than fullerenes because NFAs can generate more excitons and can have intrinsically higher hole mobility. Additionally, pairing NFAs with a donor that forms a small HOMO offset will minimize hole trapping, further increasing photocurrent generation.

https://doi.org/10.1021/acs.jpcc.2c07821
J. Phys. Chem. C 2022, 126, 20793−20799

■ ASSOCIATED CONTENT

Supporting Information

The Supporting Information is available free of charge at https://pubs.acs.org/doi/10.1021/acs.jpcc.2c07821.

Complex optical constants and generation rate profiles of DD devices, GIXRD patterns, capacitance versus voltage curves to obtain relative permittivity (ε_r) of DD devices, example $J-V$ curves of hole-only DD devices used in SCLC fitting to obtain μ_h, absorbance, photoluminescence, energy levels of neat materials, and $J_{ph}-V_{eff}$ data for charge collection (PDF)

■ AUTHOR INFORMATION

Corresponding Author

Julia W. P. Hsu − *Department of Materials Science and Engineering, University of Texas at Dallas, Richardson, Texas 75080, United States;* orcid.org/0000-0002-7821-3001; Email: jwhsu@utdallas.edu

Authors

Boya Zhang − *Department of Materials Science and Engineering, University of Texas at Dallas, Richardson, Texas 75080, United States*

Justin C. Bonner − *Department of Materials Science and Engineering, University of Texas at Dallas, Richardson, Texas 75080, United States*

Weijie Xu − *Department of Materials Science and Engineering, University of Texas at Dallas, Richardson, Texas 75080, United States;* orcid.org/0000-0002-4198-7265

Robert T. Piper − *Department of Materials Science and Engineering, University of Texas at Dallas, Richardson, Texas 75080, United States;* orcid.org/0000-0002-4032-0602

Lakshmi N. S. Murthy − *Department of Materials Science and Engineering, University of Texas at Dallas, Richardson, Texas 75080, United States*

Complete contact information is available at: https://pubs.acs.org/10.1021/acs.jpcc.2c07821

Notes

The authors declare no competing financial interest.

■ ACKNOWLEDGMENTS

The authors thank Prof. Wallace for the use of the spectroscopic ellipsometer and M. Herrera Lara, B. Bhandari, and J. L. Grayson for their assistance in experimental measurements. This project is supported by the National Science Foundation (CBET-1916612). J.W.P.H. acknowledges the Texas Instruments Distinguished Chair in Nanoelectronics.

■ REFERENCES

(1) Zhang, M.; Wang, H.; Tian, H.; Geng, Y.; Tang, C. W. Bulk Heterojunction Photovoltaic Cells with Low Donor Concentration. *Adv. Mater.* **2011**, *23*, 4960−4964.

(2) Yang, B.; Xiao, Z.; Huang, J. Polymer Aggregation Correlated Transition from Schottky-Junction to Bulk Heterojunction Organic Solar Cells. *Appl. Phys. Lett.* **2014**, *104*, 143304.

(3) Vandewal, K.; Widmer, J.; Heumueller, T.; Brabec, C. J.; McGehee, M. D.; Leo, K.; Riede, M.; Salleo, A. Increased Open-Circuit Voltage of Organic Solar Cells by Reduced Donor-Acceptor Interface Area. *Adv. Mater.* **2014**, *26*, 3839−3843.

(4) Ding, K.; Liu, X.; Forrest, S. R. Charge Transfer and Collection in Dilute Organic Donor-Acceptor Heterojunction Blends. *Nano Lett.* **2018**, *18*, 3180−3184.

(5) Zheng, Y. Q.; Potscavage, W. J.; Komino, T.; Hirade, M.; Adachi, J.; Adachi, C. Highly Efficient Bulk Heterojunction Photovoltaic Cells Based on C 70 and Tetraphenyldibenzoperiflanthene. *Appl. Phys. Lett.* **2013**, *102*, 143304.

(6) Murthy, L. N. S.; Kramer, A.; Zhang, B.; Su, J. M.; Chen, Y. S.; Wong, K. T.; Vandenberghe, W. G.; Hsu, J. W. P. Energy Levels in Dilute-Donor Organic Solar Cell Photocurrent Generation: A Thienothiophene Donor Molecule Study. *Org. Electron.* **2021**, *92*, 106137.

(7) Albes, T.; Xu, L.; Wang, J.; Hsu, J. W. P.; Gagliardi, A. Origin of Photocurrent in Fullerene-Based Solar Cells. *J. Phys. Chem. C* **2018**, *122*, 15140−15148.

(8) Xu, L.; Wang, J.; Villa, M.; Daunis, T. B.; Lee, Y. J.; Malko, A. V.; Hsu, J. W. P. Quantitative Analyses of Competing Photocurrent Generation Mechanisms in Fullerene-Based Organic Photovoltaics. *J. Phys. Chem. C* **2016**, *120*, 16470−16477.

(9) Kaiser, W.; Murthy, L. N. S.; Chung, C.; Wong, K.; Hsu, J. W. P.; Gagliardi, A. Origin of Hole Transport in Small Molecule Dilute Donor Solar Cells. *Adv. Energy Sustain. Res.* **2021**, *2*, 2000042.

(10) Seo, J. W.; Kim, J. H.; Kim, M.; Jin, S. M.; Lee, S. H.; Cho, C.; Lee, E.; Yoo, S.; Park, J. Y.; Lee, J. Y. Columnar-Structured Low-Concentration Donor Molecules in Bulk Heterojunction Organic Solar Cells. *ACS Omega* **2018**, *3*, 929−936.

(11) Melianas, A.; Pranculis, V.; Spoltore, D.; Benduhn, J.; Inganäs, O.; Gulbinas, V.; Vandewal, K.; Kemerink, M. Charge Transport in Pure and Mixed Phases in Organic Solar Cells. *Adv. Energy Mater.* **2017**, *7*, 1700888.

(12) He, Y.; Li, Y. Fullerene Derivative Acceptors for High Performance Polymer Solar Cells. *Phys. Chem. Chem. Phys.* **2011**, *13*, 1970−1983.

(13) Cheng, P.; Li, G.; Zhan, X.; Yang, Y. Next-Generation Organic Photovoltaics Based on Non-Fullerene Acceptors. *Nat. Photonics* **2018**, *12*, 131−142.

(14) Zhang, G.; Chen, X.-K.; Xiao, J.; Chow, P. C. Y.; Ren, M.; Kupgan, G.; Jiao, X.; Chan, C. C. S.; Du, X.; Xia, R.; et al. Delocalization of Exciton and Electron Wavefunction in Non-Fullerene Acceptor Molecules Enables Efficient Organic Solar Cells. *Nat. Commun.* **2020**, *11*, 3943.

(15) Liu, Y.; Zhang, J.; Zhou, G.; Liu, F.; Zhu, X.; Zhang, F. Electric Field Facilitating Hole Transfer in Non-Fullerene Organic Solar Cells with a Negative HOMO Offset. *J. Phys. Chem. C* **2020**, *124*, 15132−15139.

(16) Yao, N.; Wang, J.; Chen, Z.; Bian, Q.; Xia, Y.; Zhang, R.; Zhang, J.; Qin, L.; Zhu, H.; Zhang, Y.; et al. Efficient Charge Transport Enables High Efficiency in Dilute Donor Organic Solar Cells. *J. Phys. Chem. Lett.* **2021**, *12*, 5039−5044.

(17) Xue, J.; Naveed, H. B.; Zhao, H.; Lin, B.; Wang, Y.; Zhu, Q.; Wu, B.; Bi, Z.; Zhou, X.; Zhao, C.; et al. Kinetic Processes of Phase Separation and Aggregation Behaviors in Slot-Die Processed High Efficiency Y6-Based Organic Solar Cells. *J. Mater. Chem. A* **2022**, *10*, 13439−13447.

(18) Jasiūnas, R.; Zhang, H.; Devižis, A.; Franckevičius, M.; Gao, F.; Gulbinas, V. Thermally Activated Reverse Electron Transfer Limits Carrier Generation Efficiency in PM6:Y6 Non-Fullerene Organic Solar Cells. *Sol. RRL* **2022**, *6*, 2100963.

(19) Yu, K.; Song, W.; Ge, J.; Zheng, K.; Xie, L.; Chen, Z.; Qiu, Y.; Hong, L.; Liu, C.; Ge, Z. 18.01% Efficiency Organic Solar Cell and 2.53% Light Utilization Efficiency Semitransparent Organic Solar Cell Enabled by Optimizing PM6:Y6 Active Layer Morphology. *Sci. China: Chem.* **2022**, *65*, 1615−1622.

(20) Xie, L.; Zhang, Y.; Zhuang, W.; Jeong, S. Y.; Bian, Q.; Li, H.; Cao, J.; Liu, W.; Tan, H.; Woo, H. Y.; et al. Low-Bandgap Nonfullerene Acceptor Based on Thieno[3,2-b]Indole Core for Highly Efficient Binary and Ternary Organic Solar Cells. *Chem. Eng. J.* **2022**, *427*, 131674.

(21) Zhang, L.; Zhao, H.; Hu, M.; Wang, X.; Hu, L.; Mao, H.; Yuan, Z.; Ma, W.; Chen, Y. Enhanced Efficiency and Excellent Thermostability in Organic Photovoltaics via Ternary Strategy with Twisted Conjugated Compound. *Small* **2021**, *17*, 2103537.
(22) Li, P.; Fang, J.; Wang, Y.; Manzhos, S.; Cai, L.; Song, Z.; Li, Y.; Song, T.; Wang, X.; Guo, X.; et al. Synergistic Effect of Dielectric Property and Energy Transfer on Charge Separation in Non-Fullerene-Based Solar Cells. *Angew. Chem., Int. Ed.* **2021**, *60*, 15054−15062.
(23) Cui, C. Recent Progress in Fused-Ring Based Nonfullerene Acceptors for Polymer Solar Cells. *Front. Chem.* **2018**, *6*, 1−11.
(24) Du, J.; Fortney, A.; Washington, K. E.; Biewer, M. C.; Kowalewski, T.; Stefan, M. C. Benzo[1,2-: B:4,5- b′]Difuran and Furan Substituted Diketopyrrolopyrrole Alternating Copolymer for Organic Photovoltaics with High Fill Factor. *J. Mater. Chem. A* **2017**, *5*, 15591−15600.
(25) Du, J.; Bulumulla, C.; Mejia, I.; McCandless, G. T.; Biewer, M. C.; Stefan, M. C. Evaluation of (E)-1,2-Di(Furan-2-Yl)Ethene as Building Unit in Diketopyrrolopyrrole Alternating Copolymers for Transistors. *Polym. Chem.* **2017**, *8*, 6181−6187.
(26) Wang, Q. Solution-Processed Small-Molecule Organic Solar Cells. Ph.D. Thesis, Technische Universiteit Eindhoven, 2017.
(27) Zhang, B.; Murthy, L. N. S.; Mishra, A.; Bowler, M. H.; Chung, C.-L.; Du, J.; Stefan, M. C.; Wong, K.-T.; Slinker, J. D.; Hsu, J. W. P. Re-Examining Open-Circuit Voltage in Dilute-Donor Organic Photovoltaics. *J. Phys. Chem. C* **2022**, *126*, 9275−9283.
(28) Hussain, K.; Kaiser, W.; Gagliardi, A. Effect of Polymer Morphology on Dilute Donor Organic Solar Cells. *J. Phys. Chem. C* **2020**, *124*, 3517−3528.
(29) Burkhard, G. F.; Hoke, E. T.; McGehee, M. D. Accounting for Interference, Scattering, and Electrode Absorption to Make Accurate Internal Quantum Efficiency Measurements in Organic and Other Thin Solar Cells. *Adv. Mater.* **2010**, *22*, 3293−3297.
(30) Pettersson, L. A. A.; Roman, L. S.; Inganäs, O. Modeling Photocurrent Action Spectra of Photovoltaic Devices Based on Organic Thin Films. *J. Appl. Phys.* **1999**, *86*, 487−496.
(31) Lee, T.; Sanzogni, A.; Zhangzhou, N.; Burn, P. L.; Mark, A. E. Morphology of a Bulk Heterojunction Photovoltaic Cell with Low Donor Concentration. *ACS Appl. Mater. Interfaces* **2018**, *10*, 32413−32419.
(32) Zhu, W.; Spencer, A. P.; Mukherjee, S.; Alzola, J. M.; Sangwan, V. K.; Amsterdam, S. H.; Swick, S. M.; Jones, L. O.; Heiber, M. C.; Herzing, A. A.; et al. Crystallography, Morphology, Electronic Structure, and Transport in Non-Fullerene/Non-Indacenodithienothiophene Polymer:Y6 Solar Cells. *J. Am. Chem. Soc.* **2020**, *142*, 14532−14547.
(33) Blakesley, J. C.; Castro, F. A.; Kylberg, W.; Dibb, G. F. A.; Arantes, C.; Valaski, R.; Cremona, M.; Kim, J. S.; Kim, J. S. Towards Reliable Charge-Mobility Benchmark Measurements for Organic Semiconductors. *Org. Electron.* **2014**, *15*, 1263−1272.
(34) Zhang, X.; Yao, N.; Wang, R.; Li, Y.; Zhang, D.; Wu, G.; Zhou, J.; Li, X.; Zhang, H.; Zhang, J.; et al. On the Understanding of Energy Loss and Device Fill Factor Trade-Offs in Non-Fullerene Organic Solar Cells with Varied Energy Levels. *Nano Energy* **2020**, *75*, 105032.
(35) Ratcliff, E. L.; Zacher, B.; Armstrong, N. R. Selective Interlayers and Contacts in Organic Photovoltaic Cells. *J. Phys. Chem. Lett.* **2011**, *2*, 1337−1350.

https://doi.org/10.1021/acs.jpcc.2c07821
J. Phys. Chem. C 2022, 126, 20793−20799